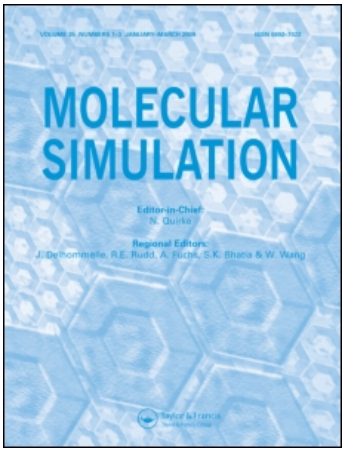

Molecular Simulation
Publication details, including instructions for authors and subscription information:
http://www.informaworld.com/smpp/title~content=t713644482

A Comparison of Non-Bonded Scaling Approaches for Free Energy Calculations

Jed W. Pitera[a]; Wilfred F. van Gunsteren[a]
[a] Laboratory of Physical Chemistry, Swiss Federal Institute of Technology, Zürich, Switzerland

Online publication date: 26 October 2010

To cite this Article Pitera, Jed W. and van Gunsteren, Wilfred F.(2002) 'A Comparison of Non-Bonded Scaling Approaches for Free Energy Calculations', Molecular Simulation, 28: 1, 45 — 65
To link to this Article: DOI: 10.1080/08927020211973
URL: http://dx.doi.org/10.1080/08927020211973

Molecular Simulation, 2002, Vol. 28(1–2), pp. 45–65

Taylor & Francis
Taylor & Francis Group

A COMPARISON OF NON-BONDED SCALING APPROACHES FOR FREE ENERGY CALCULATIONS

JED W. PITERA and WILFRED F. VAN GUNSTEREN*

Laboratory of Physical Chemistry, Swiss Federal Institute of Technology, ETH Zürich, ETH Zentrum, CH-8092 Zürich, Switzerland

(Received August 2000; accepted December 2000)

One of the long-standing problems in free energy calculations that involve the annihilation of particles is the choice of how to scale the non-bonded interactions of the disappearing particle. We make use of a "null transformation" (converting naphthalene to naphthalene) to extensively test and compare a number of scaling approaches, including simple linear, quadratic, mixed non-linear and separation-shifted ("soft-core") scaling. While any protocol that involves some sort of non-linear scaling yields reasonable free energy results, only the "soft-core" scaling methods yield completely stable dynamics near the simulation end-points. Additional advantages of this method in the context of complex molecular conversions are also discussed.

Keywords: Free energy calculations; Molecular dynamics; Thermodynamic integration; Non-bonded interactions; End-point catastrophe

INTRODUCTION

Free energy calculations provide a direct and valuable connection between the microscopic world of computer simulation and the macroscopic world of experimental observables. The result from a free energy calculation – the relative free energy of two related systems – is directly comparable to the relative free energy of those two systems as measured experimentally. Numerous reviews [1, 2, 3] have detailed the application of free energy calculations to diverse systems of chemical or biochemical interest. In this

*Corresponding author. Tel.: +41-1-632-5501, Fax: +41-1-632-1039, e-mail: wfvgn@igc.phys. chem.ethz.ch

ISSN: 0892-7022 DOI: 10.1080/08927020290004368

work, we are solely concerned with transformational or "alchemical" free energy calculations [4] that compare the free energy of two chemically distinct systems rather than conformational free energy calculations which aim to compare the free energies of different conformations of the same system.

In the realm of biomolecular simulation, there are two primary methods used to calculate the relative free energy of two different chemical species: free energy "perturbation" (FEP) [5] and thermodynamic integration (TI) [6]. Both approaches make substantial use of a coupling parameter formalism [7], where an artificial coordinate is used to connect the two systems of interest along a non-physical path. The coupling parameter, typically called λ, is used to smoothly transform the simulated system between the two real systems – or "end states" of interest ("A" and "B" in our nomenclature, which correspond to $\lambda = 0$ and $\lambda = 1$, respectively). In FEP the free energy difference between systems A and B is determined by

$$\Delta G(A \rightarrow B) = -kT \ln \langle e^{-(H_B - H_A)/kT} \rangle_A \tag{1}$$

where the necessary ensemble average only involves the simulation of state A. In practice, this is broken up into a number of sub-simulations which each calculate the free energy difference between adjacent fractional values of λ, and the overall result is obtained by summation. In contrast, TI makes use of the fact that the free energy change along λ can be expressed as

$$\Delta G(0 \rightarrow 1) = \int_0^1 \left\langle \frac{\partial H}{\partial \lambda} \right\rangle_\lambda d\lambda \tag{2}$$

Typically, the integrand in Eq. (2) is not linear, and simulations at a number of points on the $\lambda = 0,1$ interval are required to accurately determine ΔG. Though the ensemble averages required for both FEP and TI have been expressed in terms of the Hamiltonian, we have only investigated the effect of several approaches for scaling the potential energy of the system between its two end states. To simplify the discussion, the remaining equations will describe various forms of scaling in terms of $V(\lambda)$, but the actual calculation makes use of $H(\lambda)$. In general, TI calculations are now preferred to FEP calculations for transformations in complex mixed

systems, such as protein-ligand complexes. Consequently, we will concentrate on TI calculations in this work, though some of our observations are germane to FEP methods as well.

For all their power, there are still significant technical challenges that limit the accuracy and utility of free energy calculations. When the two systems of interest differ in the number of atoms, it is necessary that some atoms from the larger system be converted to non-interacting "dummy" particles over the course of the calculation. This is typically done by scaling their non-bonded (van der Waals and electrostatic) interactions to zero as a function of the coupling parameter. In the simple (linear) case of a particle that disappears in state B, this becomes:

$$V(\lambda) = (1 - \lambda) \cdot V_A + \lambda \cdot 0 \tag{3}$$

However straightforward this seems, the nature of the van der Waals interaction itself generates additional complexity. The true quantum-mechanical interatomic potential is typically approximated in molecular mechanics models by the combination of three terms: charge–charge Coulomb interaction (r^{-1}); induced-dipole dispersion or van der Waals attraction (r^{-6}); and electron–electron exchange repulsion (r^{-12} or e^{-r}). The attractive r^{-6} and repulsive r^{-12} terms correspond to the Lennard-Jones potential commonly used in biomolecular simulation. The repulsive exchange term dominates at short distances, and yields a positive singularity at the origin. This repulsive "hard core" causes particular problems for free energy calculations where particles disappear. Figure 1a shows the standard GROMOS96 Lennard-Jones potential energy term between a water oxygen atom and an aromatic CH atom. The effects of simple linear scaling (Eq. (3)) on this potential energy term are shown in Figure 1b. At $\lambda = 1$, the potential is zero everywhere. Any smaller value of λ (0.99999, for example) yields the repulsive singularity at the origin.

In general, there are two problems associated with the creation or annihilation of particles in molecular simulation. First, the scaled potential must permit a stable simulation. This is primarily an issue for molecular dynamics, where the rapidly changing forces associated with the "hard cores" of appearing particles cause difficulty in integrating the equations of motion, an effect commonly known as the "end-point catastrophe" [2, 3]. However, it is also present in all simulations in a more subtle way – as the non-ergodicity that arises when solvent molecules get trapped or distorted by a "cage" of repulsive dummy particles as these appear. Without a

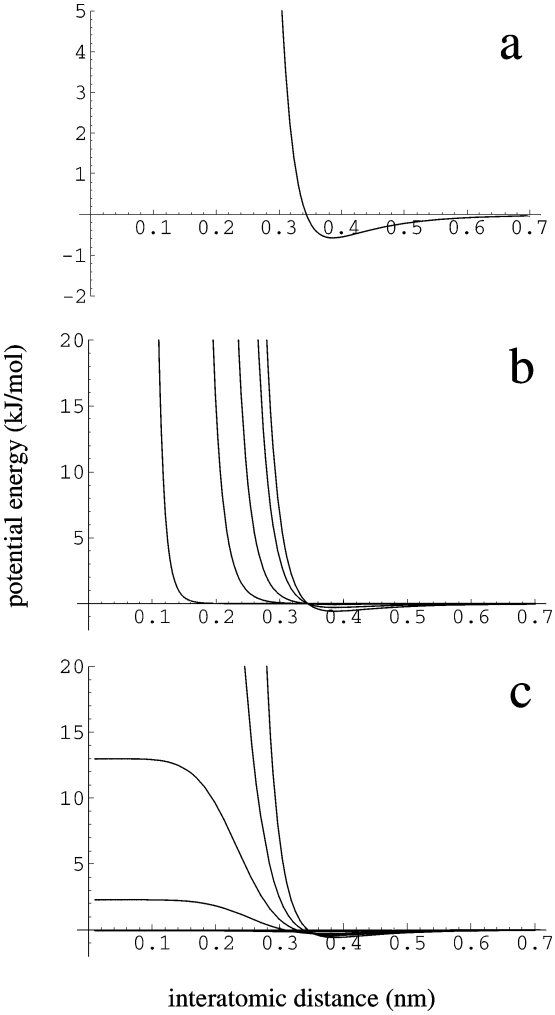

FIGURE 1 A comparison of the Lennard-Jones van der Waals potential energy term from the GROMOS96 force field [22] for the interaction of a water oxygen (OW) with an aromatic united atom carbon (CH). Figure 1a shows the normal (unscaled) interaction. In Figure 1b, the effect of linearly scaling the interaction to zero as a function of the coupling parameter λ is displayed for $\lambda = 0, 0.5, 0.9, 0.99$ and 0.99999. The different curves correspond to different λ values. Figure 1c shows a linear soft-core scaling of the same interaction, as described in the text, with a soft-core scaling parameter of $\alpha_{LJ} = 2.0$. Curves are graphed for $\lambda = 0$, 0.25, 0.375, 0.5 and 0.75.

stable simulation, it is impossible to calculate the ensemble averages necessary for the calculation of a free energy. The second issue is the integrability of the ensemble averages themselves. As noted, a TI

calculation is typically broken into sub-simulations at a number of λ values. To maximize the accuracy of the calculation, the integrand should be as smooth (*i.e.*, have the smallest second derivatives) as possible on the path connecting the two end states. Furthermore, the statistical uncertainty of the ensemble average $\langle \partial \mathrm{H}/\partial\lambda \rangle$ should ideally be similar and small at every λ value. This latter property is especially important since it permits efficient parallelization of the calculation by assigning simulations at different λ values to different processors, avoiding the need for complex load balancing.

Of the two problems we have mentioned, the first (simulation stability) has understandably received more attention in the literature. Historically, the simplest method of addressing this problem is by avoiding it – that is, by not simulating λ values near the end states but simply extrapolating the results from simulations at stable λ values [8]. To some extent, this is implicitly done in so-called "slow growth" calculations, which continuously shift the value of λ over the course of a single simulation and thus spend very little time sampling problematic regions of λ space. Unfortunately, "slow growth" calculations have a number of well-known problems themselves [9]. A second approach is to "hide" the tiny repulsive singularities of any appearing particles within the thermal radius of adjacent atoms (whose properties do not vary with λ) until the nascent particles are large enough not to disturb the calculation. In practice, this is done through "bond-shrink" or "shrink" methods [10], which reduce the length of bonds to dummy particles to infinitesimal values (typically 0.01 nm) and scale them to their equilibrium lengths as the particles appear. A third approach, which does not require any changes to the equilibrium geometry of the simulated species and removes, rather than avoids, the dynamical instability associated with disappearing particles is the "soft-core" or "separation-shifted scaling" approach [11, 12]. Simply, this scaling method adds a λ-dependent offset to the interatomic distance used in the non-bonded potential energy calculations, and thus avoids the problematic singularity:

$$V_{A,soft}(r, \lambda, \alpha_{LJ}, \alpha_C) = \frac{C12_A}{(r^6 + \lambda^2 \cdot \alpha_{LJ} \cdot (C12_A/C6_A))^2} - \frac{C6_A}{(r^6 + \lambda^2 \cdot \alpha_{LJ} \cdot (C12_A/C6_A))} + \frac{q_{i,A} q_{j,A}}{4\pi\varepsilon_0 \sqrt{r^2 + \lambda^2 \cdot \alpha_C}} \quad (4)$$

Note that this still requires some sort of interpolation of the simulated Hamiltonian between the two end states:

$$V(\lambda) = (1 - \lambda) \cdot V_{A,soft} + \lambda \cdot 0 \tag{5}$$

At short interatomic distances, the singularity is smoothly replaced by the energy of interaction at a minimum effective distance r_{eff} which corresponds to

$$r_{\text{eff}} = \sqrt[6]{\lambda^2 \cdot \alpha_{LJ} \cdot \frac{C12_A}{C6_A}} \tag{6}$$

where α_{LJ} is an adjustable parameter. This scaling protocol has successfully been used in a number of cases, including the solvation free energies of tryptophan analogs [13] and the relative binding free energies of estrogen-like compounds [14] to their receptor. Its effects in a typical non-bonded interaction can be clearly seen in Figure 1c, which as before shows the non-bonded interaction between a water oxygen and a CH united atom aromatic carbon as a function of distance and λ.

Separate from the issue of dynamical stability is the issue of integrability. That is, regardless of how well the underlying simulation behaves, how precise is the calculated free energy? Along with the "end-point" catastrophe in dynamics comes an "integrand catastrophe". Namely, with simple linear scaling the value of $\langle \partial H/\partial \lambda \rangle$ is many orders of magnitude larger at the $\lambda = 0$ or $\lambda = 1$ end points than at nearby values of λ (0.05, for example). As a result, the calculated free energy is entirely dominated by these values, and the statistical uncertainty is concentrated in a single section of the integration. Unfortunately, this problem cannot be avoided by simply performing extensive simulations of the two end states and avoiding intermediate λ values, due to the typical non-linearity of $\langle \partial H/\partial \lambda \rangle$ as a function of the coupling parameter [15]. An early protocol suggested to avoid this problem was to make the mixed potential a non-linear function of λ [16]:

$$V(\lambda) = (1 - \lambda)^n \cdot V_A + \lambda^n \cdot 0 \tag{7}$$

A similar method simply uses linear scaling and increases the density of simulated λ values near problematic regions like the end states. While this is straightforward and somewhat effective at addressing the integrability problem, it suffers from the dynamical instabilities noted

above. Additionally, for real-world calculations it is impossible to know *a priori* which regions of λ will be problematic. This makes such methods difficult to automate or parallelize efficiently. A more general approach is to adopt a different λ-dependence for different terms of the non-bonded interaction [17]:

$$V_A(r;\lambda) = (1-\lambda)^l \frac{C12_A}{r^{12}} - (1-\lambda)^m \frac{C6_A}{r^6} + (1-\lambda)^n \frac{q_{i,A}q_{j,A}}{4\pi\varepsilon_0 r} \tag{8}$$

where common choices for the powers l, m and n are 3, 5 and 3 respectively [18, 19]. While this serves the purpose of more evenly distributing the change in the integrand, it still suffers from dynamical instabilities near the end points of the calculation, which are typically avoided by using a "bond-shrink" protocol. The only methods so far described which solve both problems – by producing stable dynamics and simultaneously yielding a smooth integrand – are derivatives of the soft-core scaling [11] previously mentioned. In the present work we evaluate both linear (Eq. (5)) and quadratic soft-core protocols:

$$V(\lambda) = (1-\lambda)^2 \cdot V_{A,soft} + \lambda^2 \cdot 0 \tag{9}$$

As noted, the choice of correct protocol is often highly system-dependent. Unfortunately, there are only a few detailed comparisons of several different non-bonded scaling protocols applied to the same system available in the literature [18, 20]. Inspired by the work of Pearlman [21], we have selected a "null transformation" – where one molecule is transformed into a symmetry-related twin of itself as a function of λ – to provide a test case for these disparate non-bonded scaling protocols. "Null transformations" have the advantage that their correct free energy difference is rigorously zero, regardless of the potential function or simulation parameters used. Accordingly, we have tested six different commonly used scaling protocols with a simple simulation protocol for the transformation of napthalene into napthalene ($\Delta G = 0$), and assessed their ability to address both of the problems noted above. The protocols we have tested include simple linear scaling ("H", Eq. (3)), simple quadratic scaling ("H2", Eq. (7) with $n = 2$), soft-core scaling ("S", Eq. (5)), quadratic soft-core scaling ("S2", Eq. (9)), simple linear scaling with shrinking bonds ("H shrink", Eq. (3) with shrinking bonds), and mixed non-linear scaling with shrinking bonds ("H3,5,3 shrink", Eq. (8) with $l = 3$, $m = 5$, $n = 3$ and shrinking bonds).

SYSTEMS AND METHODS

All calculations were carried out with the united atom "naphthalene" solute shown in Figure 2, using the GROMOS96 force field [22] and simulation software [23]. An additional "dummy" anthracene-like aromatic ring allows this solute to be converted between two distinct naphthalene molecules. The non-bonded atom types and van der Waals parameters for these two end-states are listed in Table I. All solute atoms were uncharged. Bond, bond-angle and improper dihedral terms were typically the same in both end states, with the exception of the two "bond-shrink" calculations. All bonds had an equilibrium length of 0.139 nm and a force constant of $1.08 * 10^7$ kJ/mol nm^{-4} (GROMOS96 bond type 15), while bond-angle terms had an equilibrium angle of 120 degrees and a force constant of 560 kJ/mol. Since the solute is rigidly planar, there are no torsional dihedrals, while the planarity is enforced by improper dihedral force field terms with a force

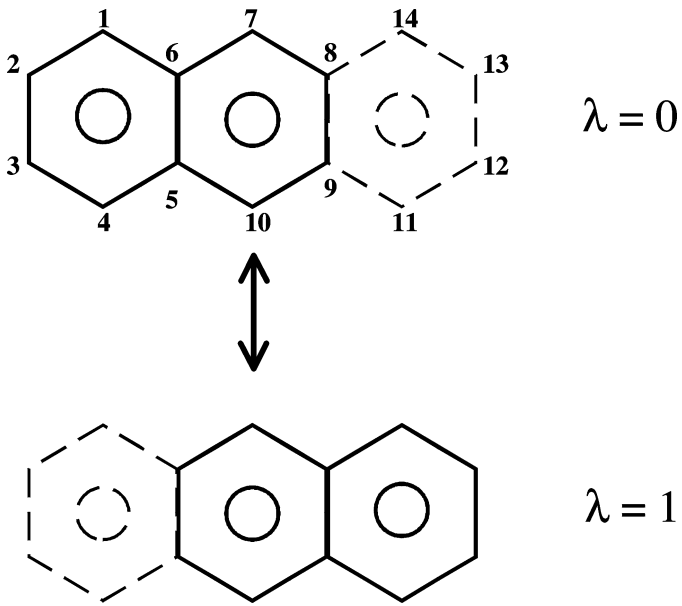

FIGURE 2 The "naphthalene" solute used for the free energy calculations. The upper molecule is the $\lambda = 0$ or "A" state, where the ring on the right side of the molecule consists of non-interacting dummy atoms. The calculations consisted of converting this species to the one below it ($\lambda = 1$ or "B"), where the right-hand ring is now a fully interacting aromatic ring and the left-hand ring has been converted to dummy atoms. Since these two species are symmetry-related, the free energy difference between them is rigorously zero. Atom numbers for reference to Table I are shown in the "A" state only, but apply for both states.

TABLE I Atom information for the two end states ("A" or $\lambda = 0$ and "B" or $\lambda = 1$) of the united atom pseudo-naphthalene solute used in all free energy calculations in this paper. Atom numbers refer to the molecular structures shown in Figures 2 and 3. The parameters corresponding to each GROMOS96 integer atom code are detailed in Table II

	State A ($\lambda = 0$)		*State B* ($\lambda = 1$)	
Atom number	*Atom type*	*GROMOS96 integer atom code*	*Atom type*	*GROMOS96 integer atom code*
1,2,3,4	CH	16	Dummy	19
5,6	C	11	CH	16
7,10	CH	16	CH	16
8,9	CH	16	C	11
11,12,13,14	Dummy	19	CH	16

constant of 0.051 kJ/mol degree^{-1} and an equilibrium angle of 0 degrees. There are six improper dihedral angles per ring and an additional one for each atom that joins two rings [22]. Intrasolute non-bonded interactions were not calculated between atoms separated by fewer than 4 bonds. In the two "bond-shrink" calculations, the bonds that form the "sides" of each ring were linearly decreased in length from their original equilibrium value of 0.139 nm to 0.01 nm as the corresponding particles disappeared, with force constants left unchanged. Figure 3 shows this process in detail.

The solute was surrounded by 1358 SPC [24] water molecules in a truncated octahedral periodic box with a minimum solute to wall distance of 1.8 nm. All simulations were carried out with a twin-range (0.8/1.4 nm) charge group cutoff for non-bonded interactions, along with a reaction field correction ($\varepsilon_{RF} = 54.0$) to minimize truncation effects [25]. A full pairlist update was carried out every 5 timesteps, while the inner (0.8 nm) pairlist was updated every timestep. The system was initially minimized for 1000 steps of steepest descent minimization at constant volume, after which initial velocities for all particles were randomly assigned from a Maxwell-Boltzmann distribution at 300 K. Subsequently, the system was equilibrated with 100 ps of constant volume and 200 ps of constant pressure (isotropic weak coupling with a coupling constant of 0.5 ps and isothermal compressibility of 0.0007624 (kJ mol^{-1} nm^{-3})$^{-1}$) molecular dynamics simulation [26]. All equilibration was carried out at $\lambda = 0$. Throughout the simulations, the temperature was maintained at the target value through weak coupling [26]. The solute and solvent were separately coupled to 300 K temperature baths with a coupling constant of 0.1 ps. Following the equilibration, all free energy calculations were carried out at constant volume. The SHAKE algorithm [27] was used with a relative tolerance of

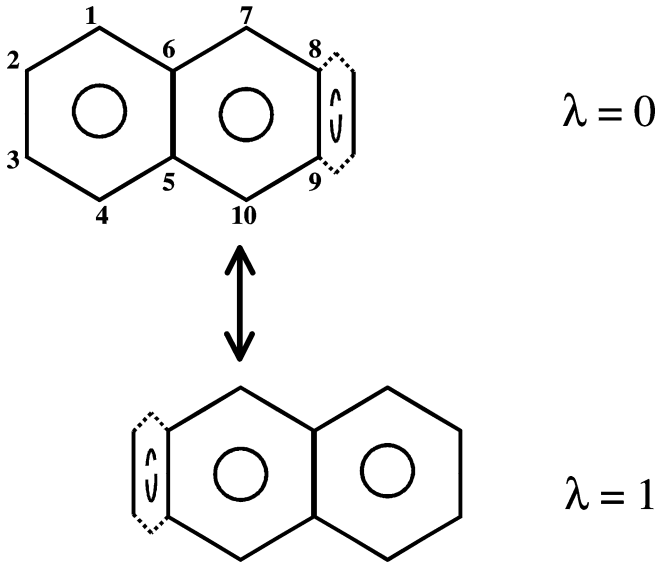

FIGURE 3 End states of the "bond-shrink" protocol used in the "H shrink" and "H3,5,3 shrink" calculations. Four of the five bonds corresponding to the dummy ring were shrunk from their normal equilibrium lengths of 0.139 nm to 0.01 nm as a linear function of λ. The force constant associated with the bond was unchanged. The upper molecule is again the $\lambda = 0$ or "A" state, which is smoothly converted to the $\lambda = 1$ or "B" state, as shown in the lower half of the figure. The atom numbering is the same as for Figure 2, but numbers for dummy atoms have been removed for clarity.

TABLE II Parameters associated with each GROMOS96 integer atom code as used in the calculations in this paper. For each atom code, the atom type, mass (in a.m.u.), attractive ($C6^{1/2}$) and repulsive ($C12^{1/2}$) Lennard-Jones parameters are detailed, along with the partial charge. For details of the potential energy function, consult Ref. [22]

*GROMOS*96 *atom code*	*Atom type*	*Mass* (*a.m.u.*)	$C6^{1/2}$ $(kJ/mol\ nm^6)^{1/2}$	$C12^{1/2}$ $(kJ/mol\ nm^{12})^{1/2}$	*Charge* (*e*)
16	CH	13.019	0.07425	0.003888	0.00
11	C	12.011	0.04838	0.001837	0.00
19	Dummy	13.019	0.00	0.00	0.00

0.00001 to constrain either all solute and solvent bond lengths to their equilibrium values (with a corresponding 2 fs timestep) or to constrain only bonds between solvent atoms (where a 1 fs timestep was used) depending on the non-bonded scaling protocol. In the latter cases it is important to note that bonds between solute atoms were not constrained with SHAKE. Due to the different timesteps used, all results are reported as a function of number of timesteps rather than simulated time.

For each non-bonded scaling protocol, an extensive series of 199 sub-simulations, each 12500 timesteps in length, were carried out. Starting at

$\lambda = 0$, simulations were carried out at 11 evenly spaced λ values from 0 to 1. An initial pass consisted of 12500 timesteps of equilibration followed by 12500 timesteps of data collection. The final configuration of this first data collection run was used as the initial configuration for equilibration at the next λ value. In this way, λ values were sampled in the "forward" direction from 0 to 1. Once $\lambda = 1$ was reached, an additional 12500 timestep equilibration at $\lambda = 1$ was run before sampling was begun in the "reverse" direction – *i.e.*, the same protocol of 12500 timesteps of equilibration followed by 12500 timesteps of data collection from 1 to 0. Once these initial "forward" and "reverse" calculations were complete, data collection was extended at each λ value (for each direction) with 7 additional runs of 12500 timesteps each. There were thus 8×12500 or 100000 timesteps of sampling per λ value in each "direction". Depending on the timestep size, this corresponds to a total simulation time of roughly 2.5 or 5.0 ns per scaling protocol. To provide a uniform basis for the comparison of the different methods, no attempts were made to optimize the number of timesteps used at each λ value or to add simulations at additional λ points in problematic regions.

As noted, a total of six different protocols for scaling of the non-bonded interactions during the free energy calculation were studied. They include simple linear scaling ("H"); simple quadratic scaling ("H2"); soft-core linear scaling ("S"); soft-core quadratic scaling ("S2"); simple linear scaling with bond shrinking ("H shrink") and mixed non-linear scaling with bond shrinking ("H3,5,3 shrink"). It was necessary to use a 1 fs timestep for all except the soft-core scaling protocols "S" and "S2" since in every other case ("H","H2","H shrink","H3,5,3 shrink") attempts to use a 2 fs timestep yielded unstable dynamics and thus failures of the SHAKE algorithm. These failures typically occurred in the simulations at λ values of 0.1 or 0.9, suggesting that they derived from collisions between solvent atoms and the repulsive cores of "appearing" solute atoms. A simulation using the "H" scaling protocol, a 1 fs timestep, and SHAKE applied to both solute and solvent bonds was also unstable, prompting the use of SHAKE solely for solvent bonds. Since the number of scaled interactions is a tiny fraction of the number of non-bonded interactions in a normal solute-solvent system, the total wall clock times for each scaling protocol are approximately identical.

RESULTS AND DISCUSSION

Figures 4 to 9 show the results of the forward and reverse TI calculations for each scaling protocol. The graphs show the value of

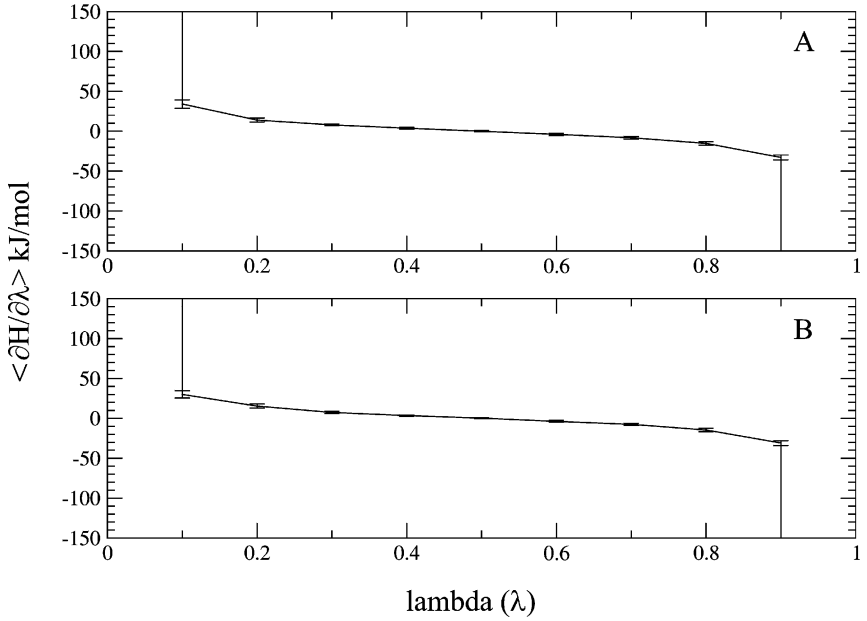

FIGURE 4 The integrand $\langle \partial H/\partial \lambda \rangle$ at each λ point for the calculation using simple linear scaling "H" of the non-bonded interactions of perturbed atoms. The curve corresponds to the block average over all 8 data collection runs (12500 timesteps each), while the error bars correspond to the standard deviation of those eight values. Graph A shows the results of the calculation in the forward direction, while the lower graph B shows the results from the reverse calculation. All values are in kJ/mol. The data point at $\lambda = 0$ or 1 is four to six orders of magnitude larger than at any other λ value and thus off the scale of these figures.

$\langle \partial H/\partial \lambda \rangle$ as a function of λ, and the values presented are the block averages over all 8 12500 timestep data collection runs, while the error bars show the standard deviation of the $\langle \partial H/\partial \lambda \rangle$ values calculated over those 8 blocks. Results for all 6 scaling protocols have been displayed at a similar scale where possible to simplify visual comparisons between the methods. For optimal integration results, the graph of $\langle \partial H/\partial \lambda \rangle$ should be relatively smooth, and the magnitude of the integrand and the standard error should be roughly uniform across λ values. In addition, the symmetry of the null transformation implies that the value of $\langle \partial H/\partial \lambda \rangle$ should be an odd function about the mid-point of the transformation at $\lambda = 0.5$. The integrated forward and reverse free energy differences are presented in Table III. A special note is necessary regarding Figure 8, which shows the results from the "H shrink" protocol. In this case, two of the eight $\lambda = 0$ reverse data collection runs

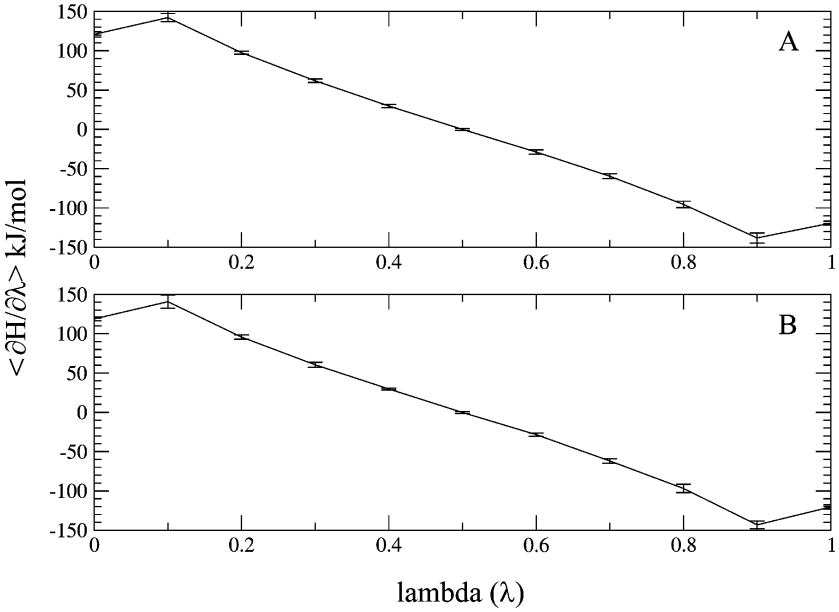

FIGURE 5 The integrand $\langle \partial H/\partial \lambda \rangle$ at each λ point for the calculation using simple quadratic scaling "H2" of the non-bonded interactions of perturbed atoms. The curve corresponds to the block average over all 8 data collection runs (12500 timesteps each), while the error bars correspond to the standard deviation of those eight values. Graph A shows the results of the calculation in the forward direction, while the lower graph B shows the results from the reverse calculation. All values are in kJ/mol.

(the fourth and fifth) experienced a very close approach of a solvent water to the particles of the shrunken dummy ring. While this was a transient collision, it caused an enormous fluctuation in the value of $\langle \partial H/\partial \lambda \rangle$ for these two runs, which deviate from those of the other six runs at this λ value by more than 10^{12} kJ/mol λ^{-1}. Consequently, data for the reverse runs of this protocol are reported both with and without results from these suspect windows. Note that Figures 7 ("S2") and 8 ("H shrink") are plotted with larger vertical scales than the other four figures in this series.

From these results it is clear that simple linear scaling ("H") does not produce a readily integrable function for $\langle \partial H/\partial \lambda \rangle$. Effectively all of the change in the integrand is restricted to the $\lambda = 0$ and $\lambda = 1$ values; upon going from $\lambda = 0$ to $\lambda = 0.1$, the integrand decreases by six orders of magnitude. This is the largest change in the derivative $\langle \partial H/\partial \lambda \rangle$ seen for any two adjacent λ windows in our calculations. The only comparable change is

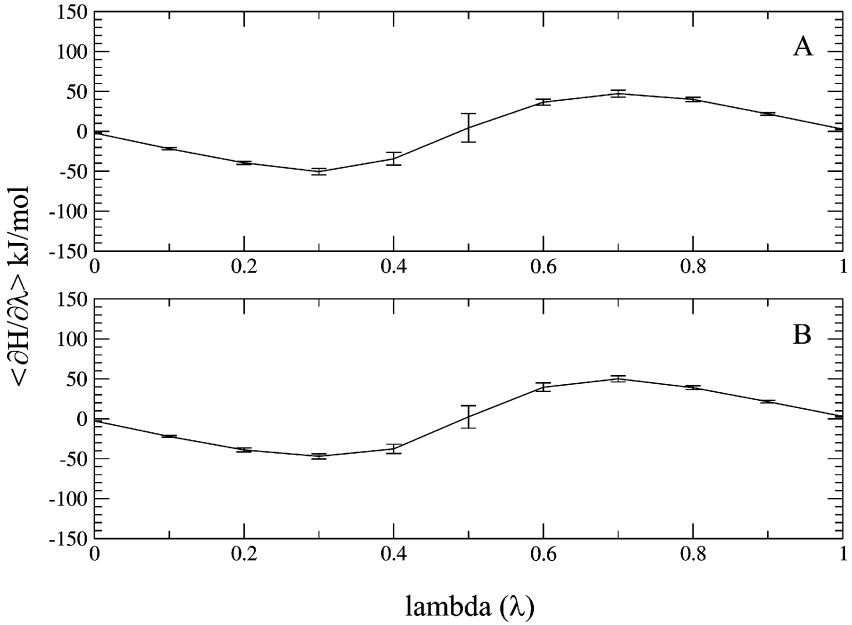

FIGURE 6 The integrand $\langle \partial H/\partial \lambda \rangle$ at each λ point for the calculation using soft-core scaling "S" of the non-bonded interactions of perturbed atoms with a scaling coefficient of $\alpha_{LJ} = 2.0$. The curve corresponds to the block average over all 8 data collection runs (12500 timesteps each), while the error bars correspond to the standard deviation of those eight values. Graph A shows the results of the calculation in the forward direction, while the lower graph B shows the results from the reverse calculation. All values are in kJ/mol.

seen with the "H shrink" method, which, as noted before, showed significant instabilities of the integrand at $\lambda = 0$. The remaining protocols ("H2", "S", "S2", and "H3,5,3 shrink") all showed relatively smooth curves for $\langle \partial H/\partial \lambda \rangle$, with statistical error somewhat evenly distributed across λ values. The "S" protocol shows a slightly increased standard deviation at $\lambda = 0.5$ relative to other values. This is due to the fact that at this point along the pathway, particles of both exterior (disappearing and appearing) rings of the solute are present as very soft, weakly interacting particles. Solvent molecules can overlap significantly with either of these rings, though there is a slight energetic penalty (see Fig. 1c).

In comparing all of these scaling methods, one essential issue is the convergence of the calculated free energy value. Figure 10 shows the convergence of the forward and reverse calculated free energies for each scaling protocol as a function of the amount of sampling per window. Dotted lines on the graphs indicate the value of kT at 300 K (2.51 kJ/mol) and clearly

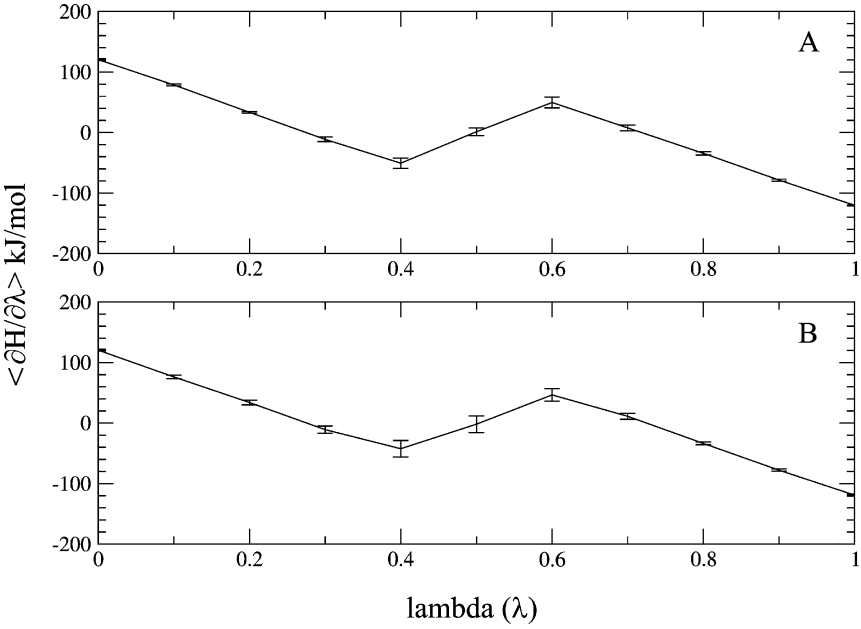

FIGURE 7 The integrand $\langle \partial H/\partial \lambda \rangle$ at each λ point for the calculation using quadratic soft-core scaling "S2" of the non-bonded interactions of perturbed atoms with a scaling coefficient of $\alpha_{LJ} = 2.0$. The curve corresponds to the block average over all 8 data collection runs (12500 timesteps each), while the error bars correspond to the standard deviation of those eight values. Graph A shows the results of the calculation in the forward direction, while the lower graph B shows the results from the reverse calculation. All values are in kJ/mol.

show that all of the higher-order scaling protocols yield calculated free energy values with an error of less than kT within 62500 timesteps of sampling per window. In fact, the "S", "S2" and "H2" methods all show errors of less than kT with only 25000 timesteps of sampling per window. Referring back to Figures 5 to 10, it is clear that these three methods show some of the smoothest $\langle \partial H/\partial \lambda \rangle$ curves. Were it not for the previously mentioned difficulties at $\lambda = 0$ with the "H shrink" protocol, it would also be an excellent choice.

An additional benefit of the soft-core scaling methods not evident in our calculations is a reduced chance for "broken ergodicity" [28]. Since interaction energies with disappearing particles smoothly scale to zero as a function of λ at all inter-particle distances, there is little chance of a solvent atom getting "trapped" or "tangled" by the nascent repulsive centers of appearing particles. Anecdotally, such problems are a common

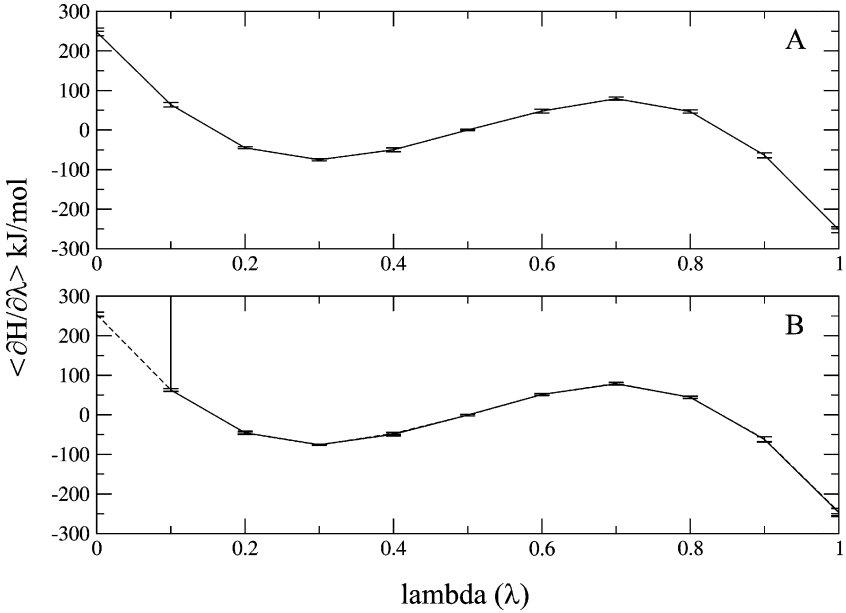

FIGURE 8 The integrand $\langle \partial H/\partial \lambda \rangle$ at each λ point for the calculation using simple linear scaling of the non-bonded interactions of perturbed atoms combined with shrinking the bonds to dummy atoms to 0.01 nm ("H shrink"). The solid curve corresponds to the block average over all 8 data collection runs (12500 timesteps each), while the error bars correspond to the standard deviation of those eight values. For the reverse run, the dotted curve and corresponding error bars show the result when two problematic runs are excluded. Graph A shows the results of the calculation in the forward direction, while the lower graph B shows the results from the reverse calculation. All values are in kJ/mol.

feature of simulations where a large number of particles appear using linear or simple non-linear scaling methods.

It should be noted that our simulated solute has no partial atomic charges. One reviewer reported some difficulty with the use of soft-core potential scaling when the "disappearing" or "appearing" atoms have partial atomic charges. Specifically, if the van der Waals repulsion is softened faster than the Coulomb interaction, catastrophes can occur where charged solvent atoms are strongly attracted to overlap the disappearing particle. In practice, this can generally be avoided by a careful choice of the α_{LJ} and α_C soft-core parameters or the use of a multi-step "electrostatic decoupling" strategy, where first the charges and then the van der Waals interactions of disappearing atoms are scaled to zero in two separate calculations.

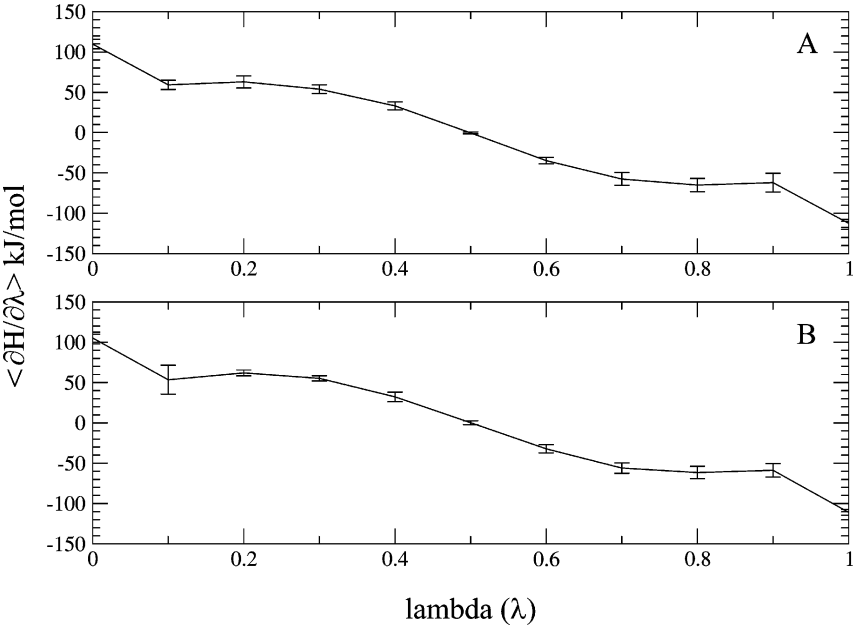

FIGURE 9 The integrand $\langle \partial H/\partial \lambda \rangle$ at each λ point for the calculation using mixed non-linear scaling of the non-bonded interactions of perturbed atoms combined with shrinking the bonds to dummy atoms to 0.01 nm ("H3,5,3 shrink"). The curve corresponds to the block average over all 8 data collection runs (12500 timesteps each), while the error bars correspond to the standard deviation of those eight values. Graph A shows the results of the calculation in the forward direction, while the lower graph B shows the results from the reverse calculation. All values are in kJ/mol.

TABLE III Final free energy values for the forward and reverse runs of each scaling protocol. These were calculated with integration by simple quadrature over the block averages of $\langle \partial H/\partial \lambda \rangle$ for the 8 12500 timestep runs at each λ point. In the case of the "H shrink" protocol, where two of the $\lambda = 0$ windows of the reverse run showed enormous values for the integrand, a second value is reported which excludes the data from those two problematic runs. The reported average is the average of forward and reverse results, while the "hysteresis" is simply half the difference of those two results. As such, it is not a true hysteresis but a lower bound on the uncertainty of the reported average value. All values are in kJ/mol, rounded to the nearest 0.1 kJ/mol

Scaling protocol	"*Forward*" *run*	"*Reverse*" *run*	*Average*	*Hysteresis*
H	$-1.1 * 10^6$	$-0.2 * 10^6$	$-0.6 * 10^6$	$0.4 * 10^6$
H2	0.9	−0.5	0.2	0.7
S	0.4	0.6	0.5	0.1
S2	−0.3	0.2	−0.1	0.3
H shrink*	0.2	$2.7 * 10^{12}$ (0.9)	$1.4 * 10^{12}$ (0.5)	$1.4 * 10^{12}$ (0.4)
H3,5,3 shrink	−1.2	−0.8	−1.0	0.2

* Values in parentheses are results when the two problematic data collection blocks are excluded.

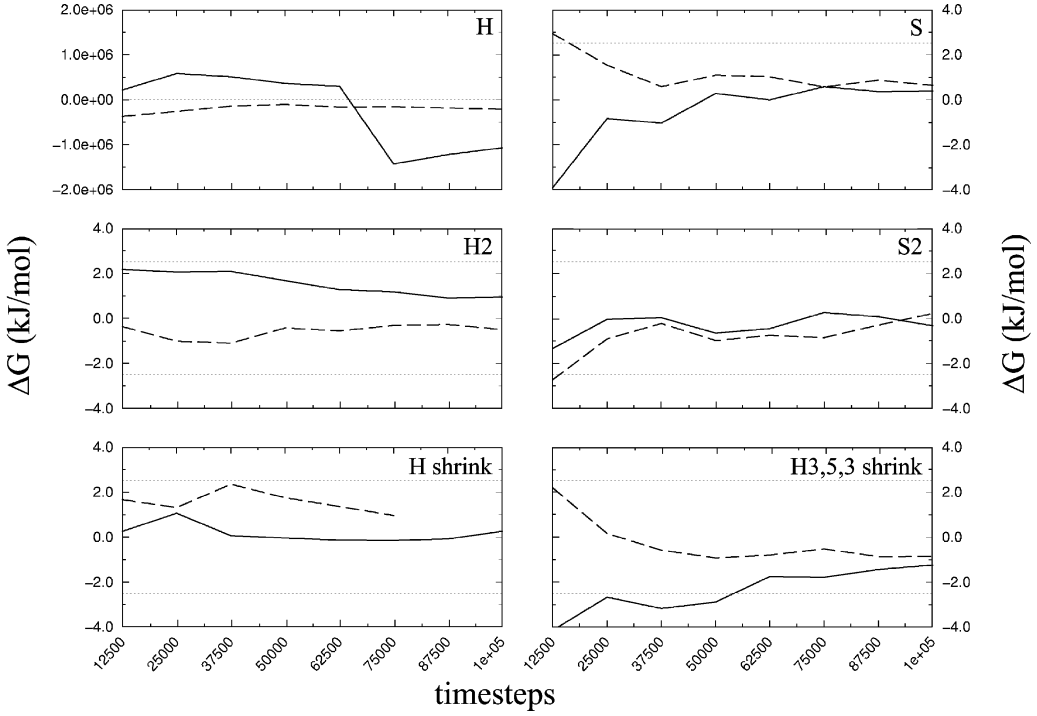

FIGURE 10 Convergence of the calculated free energy value for each scaling method as a function of the timesteps of sampling per λ point. The "forward" (solid line) and "reverse" (dashed line) calculations for each scaling protocol are shown separately. Due to the nature of the calculation, the true free energy difference is known to be rigorously 0 kJ/mol. As a guide to the eye, the light dotted lines in each graph indicate the value of $\pm$ kT at 300 K ($\pm$ 2.51 kJ/mol). Each scaling protocol is graphed in a separate panel, labeled with the name of the protocol: "H", "H2", "H shrink", "S", "S2", and "H3,5,3 shrink". Note that the vertical scales are the same for all panels except that corresponding to the "H" scaling protocol. For the reverse "H shrink" graph, data from the two runs where a solvent atom collides with a dummy atom have been excluded. All values are reported in kJ/mol.

CONCLUSIONS

Free energy calculations offer tremendous promise for the prediction of free energy differences between related systems. As the differences between systems of interest grow larger, the technical complexity of the calculation increases immensely. Techniques appropriate for calculating the relative chemical potential of two simple liquids may be inappropriate for comparing the chemical potential of two dense polymer melts, for example [29]. The fact that the free energy of a system is a state function permits the use of non-physical coupling parameter calculations like those we have studied here. However, the formal path independence of the desired result (the free energy difference) does not mean that the choice of transmutation pathway is irrelevant to the calculation. In the example we have chosen, six different possible paths are applied to a transformation with a known free energy difference. Some of these yield reasonable results, while others are clearly unacceptable without further modification. In our hands, the only protocols which yield stable dynamics with a 2 fs timestep and uniformly constrained bonds are those based on the soft-core scaling of Beutler *et al.* [11] (''S'', ''S2''). While this is not a major issue for the simple water-solvated system studied here, it is crucially important when there are slower motions and relaxation times in the system of interest, as is the case in simulations of protein-ligand complexes. The application of constraints to the intrasolute bonds might also improve the convergence of the calculation by removing some high frequency bond stretching motions that would otherwise be a source of noise. In addition to dynamical issues, the soft-core (''S'', ''S2''), and simple quadratic (''H2'') scaling methods all yield sub-kT accuracy within relatively short (25000 timestep) simulation times.

Looking to the future, the development of a simple, efficient and robust method that permits the comparison of very different molecular species is a fundamental requirement for making free energy calculations relevant to molecular design – whether it be the design of new pharmaceuticals [30], new biomolecules [31], or new materials [32]. By rigorously comparing a number of different protocols that promise this end, and identifying those that yield reliable results, we are one step closer to meeting that challenge.

Acknowledgements

JWP would like to thank the attendees of the CECAM conference ''Challenges in Free Energy Calculations'' for helpful comments.

References

[1] Kollman, P. A. (1993). "Free energy calculations: applications to chemical and biochemical phenomena", *Chem. Revs*., **93**, 2395–2417.

[2] Beveridge, D. C. and DiCapua, F. M. (1989). "Free energy *via* molecular simulation: applications to chemical and biomolecular systems", *Ann. Rev. Biophys. Biophys. Chem*., **18**, 431–492.

[3] van Gunsteren, W. F., Beutler, T. C., Fraternali, F., King, P. M., Mark, A. E. and Smith, P. E., "Computation of free energy in practice: choice of approximations and accuracy limiting factors", In: *Computer Simulation of Biomolecular Systems*, *Theoretical and "Experimental Applications*, *Volume 2*", van Gunsteren, W. F., Weiner, P. K. and Wilkinson, A. J. (Eds.), Escom Science Publishers, Leiden, 1993, pp. 182–212.

[4] Straatsma, T. P. and McCammon, J. A. (1992). "Computational alchemy", *Ann. Rev. Phys. Chem*., **43**, 407–435.

[5] Zwanzig, R. W. (1954). "High temperature equation of state by a perturbation method. I. Nonpolar gases", *J. Chem. Phys*., **22**, 1420–1426.

[6] Straatsma, T. P., Berendsen, H. J. C. and Postma, J. P. M. (1986). "Free energy of hydrophobic hydration: a molecular dynamics study of noble gases in water", *J. Chem. Phys*., **85**, 6720–6727.

[7] Chandler, D., "*Introduction to Modern Statistical Mechanics*", Oxford University Press, New York City, 1997.

[8] Lin, C. and Wood, R. H. (1994). "Free energy of solvation of a small Lennard-Jones particle", *J. Comp. Chem*., **15**, 149–154.

[9] Pearlman, D. A. and Kollman, P. A. (1989). "The lag between the Hamiltonian and the system configuration in free-energy perturbation calculations", *J. Chem. Phys*., **91**, 7831–7839.

[10] Straatsma, T. P., Zacharias, M. and McCammon, J. A. (1992). "Holonomic constraint contributions to free energy differences from thermodynamic integration molecular-dynamics simulations", *Chem. Phys. Lett*., **196**, 297–302.

[11] Beutler, T. C., Mark, A. E., van Schaik, R. C., Gerber, P. R. and van Gunsteren, W. F. (1994). "Avoiding singularities and numerical instabilities in free energy calculations based on molecular simulations", *Chem. Phys. Lett*., **222**, 529–539.

[12] Zacharias, M., Straatsma, T. P. and McCammon, J. A. (1994). "Separation-shifted scaling, a new scaling method for Lennard-Jones interactions in thermodynamic integration", *J. Chem. Phys*., **100**, 9025–9031.

[13] Daura, X., Hünenberger, P. H., Mark, A. E., Querol, E., Avilés, F. X. and van Gunsteren, W. F. (1996). "Free energies of transfer of Trp analogs from chloroform to water: comparison of theory and experiment and the importance of adequate treatment of electrostatic and internal interactions", *J. Am. Chem. Soc*., **118**, 6044–6051.

[14] Oostenbrink, C., Pitera, J. W., van Lipzig, M. M. H., Meerman, J. H. N. and van Gunsteren, W. F. (2000). "Simulations of the estrogen receptor ligand binding domain: the affinity of natural ligands and xenoestrogens", *J. Med. Chem*., **43**, 4594–4605.

[15] Radmer, R. J. and Kollman, P. A. (1997). "Free energy calculation methodology: a theoretical and empirical comparison of numerical errors and a new method for qualitative estimates of free energy changes", *J. Comp. Chem*., **18**, 902–919.

[16] Mezei, M. and Beveridge, D. L. (1986). "Free energy simulations", *Ann. NY Acad. Sci*., **482**, 1–23.

[17] Hermans, J., Yun, R. H. and Anderson, A. G. (1992). "Precision of free energies calculated by molecular dynamics simulation of peptides in solution", *J. Comp. Chem*., **13**, 429–442.

[18] Resat, H. and Mezei, M. (1993). "Studies in the free energy calculations. I. Thermodynamic integration using a polynomial path", *J. Chem. Phys*., **99**, 6052–6061.

[19] Tironi, I. G. and van Gunsteren, W. F. (1994). "A molecular dynamics simulation study of chloroform", *Mol. Phys*., **83**, 381–403.

[20] DiNola, A. and Brunger, A. T. (1998). "Free energy calculations in globular proteins", *J. Comp. Chem*., **19**, 1229–1240.

[21] Pearlman, D. A. (1994). "A comparison of alternative approaches to free energy calculations", *J. Phys. Chem*., **98**, 1487–1493.

[22] van Gunsteren, W. F., Billeter, S. R., Eising, A. A., Hünenberger, P. H., Krüger, P., Mark, A. E., Scott, W. R. P. and Tironi, I. G., Biomolecular Simulation: The GROMOS96 Manual and User Guide; Vdf Hochschulverlag AG an der ETH Zürich, Zürich, 1996.
[23] Scott, W. R. P., Hünenberger, P. H., Tironi, I. G., Mark, A. E., Billeter, S. R., Fennen, J., Torda, A. E., Huber, T., Krüger, P. and van Gunsteren, W. F. (1999). "The GROMOS biomolecular simulation program package", *J. Phys. Chem. A*, **103**, 3596–3607.
[24] Berendsen, H. J. C., Postma, J. P. M., van Gunsteren, W. F. and Hermans, J., "Interaction models for water in relation to protein hydration", In: *Intermolecular Forces*, Pullman, B. (Ed.), Reidel, Dordrecht, 1981, pp. 331–342.
[25] Tironi, I. G., Sperb, R., Smith, P. E. and van Gunsteren, W. F. (1995). "A generalized reaction field method for molecular dynamics simulations", *J. Chem. Phys.*, **102**, 5451–5459.
[26] Berendsen, H. J. C., Postma, J. P. M., van Gunsteren, W. F., DiNola, A. and Haak, J. R. (1984). "Molecular dynamics with coupling to an external bath", *J. Chem. Phys.*, **81**, 3684–3690.
[27] Ryckaert, J.-P., Ciccotti, G. and Berendsen, H. J. C. (1977). "Numerical integration of the Cartesian equations of motion of a system with constraints: molecular dynamics of n-alkanes", *J. Comp. Phys.*, **23**, 322–341.
[28] Berne, B. J. and Straub, J. E. (1997). "Novel methods of sampling phase space in the simulation of biological systems", *Curr. Opin. Struct. Biol.*, **7**, 181–189.
[29] Frenkel, D. and Smit, B., *Understanding Molecular Simulation: From Algorithms to Applications*. Academic Press, San Diego, 1996.
[30] Mark, A. E. and van Gunsteren, W. F., "Free energy calculations in drug design: a practical guide", In: *New Perspectives in Drug Design*, *Proceedings of the 9th Intl. Roundtable*, Dean, P. M., Jolies, G. and Newton, G. G. (Eds.), Academic Press, London, 1995, pp. 185–200.
[31] Harbury, P. B., Plecs, J. J., Tidor, B., Alber, T. and Kim, P. S. (1998). "High-resolution protein design with backbone freedom", *Science*, **282**, 1462–1467.
[32] Maginn, E. J., Bell, A. T. and Theodorou, D. N. (1995). "Sorption thermodynamics, siting and conformation of long n-alkanes in Silicalite as predicted by configurational-bias Monte Carlo integration", *J. Phys. Chem.*, **99**, 2057–2079.